COMPDYN 2013
4th ECCOMAS Thematic Conference on
Computational Methods in Structural Dynamics and Earthquake Engineering
M. Papadrakakis, V. Papadopoulos, V. Plevris (eds.)
Kos Island, Greece, 12–14 June 2013

TIME-DEPENDENT VULNERABILITY ASSESSMENT OF RC BUILDINGS CONSIDERING SSI AND AGING EFFECTS

Sotiria T. Karapetrou[1], Argyro M. Filippa[1], Stavroula D. Fotopoulou[1] & Kyriazis D. Pitilakis[1]

[1] Aristotle University of Thessaloniki
address
e-mail: {gkarapet,afilippa,sfotopou,kpitilak}@civil.auth.gr

Keywords: Time-dependent seismic vulnerability, RC buildings, Soil-structure interaction, Direct method, Sub-structuring method, Aging effects.

Abstract. *The present study aims at the assessment of the seismic vulnerability of reinforced concrete (RC) buildings taking into account the soil –structure –interaction (SSI) and the aging effects due to reinforcement corrosion. Two-dimensional non-linear dynamic analyses are performed to assess the seismic performance of initial (t=0 years) and 50 years old RC frame structures. Soil-structure interaction is modeled by applying the two most commonly used approaches, i.e. the substructure and the direct method, to allow for direct comparison. Chloride induced corrosion is taken into account based on probabilistic modeling of corrosion initiation time and corrosion rate. The time-dependent fragility functions are derived for predefined damage states at different time periods in terms of outcrop peak ground acceleration. The results indicate an increase of seismic vulnerability over time due to aging effects (corrosion). An overall increase in structure's fragility is also observed when considering the soil deformability and SSI. Moreover, the comparison between the two methods of SSI modeling (sub-structuring and direct) indicates the conservativeness of the sub-structuring over the direct method with the former predicting higher vulnerability compared to the later.*

1 INTRODUCTION

The seismic vulnerability of structures is commonly expressed through fragility functions, which provide the probability of exceeding prescribed levels of damage for a wide range of ground motion intensities. The assessment of the structure's seismic fragility represents a major step towards the seismic loss estimation and risk management. The soil conditions, which affect the foundation compliance, as well as the soil structure interaction, have not received much attention within the framework of structural vulnerability assessment. Although some fragility curves are available for different soil conditions taking into account the local site effects ([1]), in general, the influence of SSI effects on the seismic performance of RC structures are assumed to be beneficial and thus they are usually ignored. Nevertheless, it has been recently shown ([2], [3]) that soil deformability as well as foundation compliance may modify the structural response and fragility leading to either beneficial or unfavorable effects depending on the dynamic properties of the soil and the structure as well as the characteristics (frequency content, amplitude, significant duration) of the input motion.

In common practice it is also implicitly assumed that the structures are optimally maintained during their lifetime neglecting any deterioration mechanism which may adversely affect their structural performance. On this basis, the impact of progressive deterioration of the material properties caused by aggressive environmental attack is not accounted for. Corrosion of RC members is considered as a primary source of structural deterioration, usually associated to carbonation process and chloride penetration, leading to the variation of the mechanical properties of steel and concrete over time. Consequently, both the safety and the serviceability of RC structures may be affected under the action of seismic (or even static) loading, compromising the ability of the structures to withstand the loads they are designed for. The severe uncertainties involved in corrosion phenomena pointed out the need for a probabilistic approach to predict degradation phenomena [4]. Recognizing the importance of this issue, researchers have introduced several probabilistic models into the time-variant vulnerability assessment of corroded bridges and RC frame buildings (e.g. [5], [6], [7]).

Based on the above considerations, the aim of this study is the development of time-dependent fragility curves taking into account the SSI and aging effects. To demonstrate the methodology for the time-dependent vulnerability assessment, two reference RC moment resisting frames are selected as case studies. In total, eight structural models are analyzed based on the initial reference buildings considering (or not) the effect of SSI and aging. Soil structure interaction is studied by applying the two most commonly used methods, i.e. the sub-structuring (uncoupled) and the direct (coupled) methods, to allow for direct comparison. The direct method is based on a one-step approach where the entire soil–foundation–structure system is analyzed in a single step by a finite element model. In the substructure method, on the other hand, the SSI phenomenon is divided in two sub-domains that are finally coupled through the concept of the foundation dynamic impedance functions. The consideration of aging is achieved by including probabilistic models of chloride induced corrosion deterioration of the RC elements within the vulnerability assessment framework. Fragility curves are finally developed for the initial (t=0 years) and the corroded buildings (t=50 years) for predefined damage states based on the statistical exploitation of the results of two-dimensional nonlinear dynamic analyses of the given structures. The derived curves are compared to gain insight into the effect of SSI and reinforcement corrosion highlighting the importance of their incorporation in the vulnerability analysis (Figure 1).

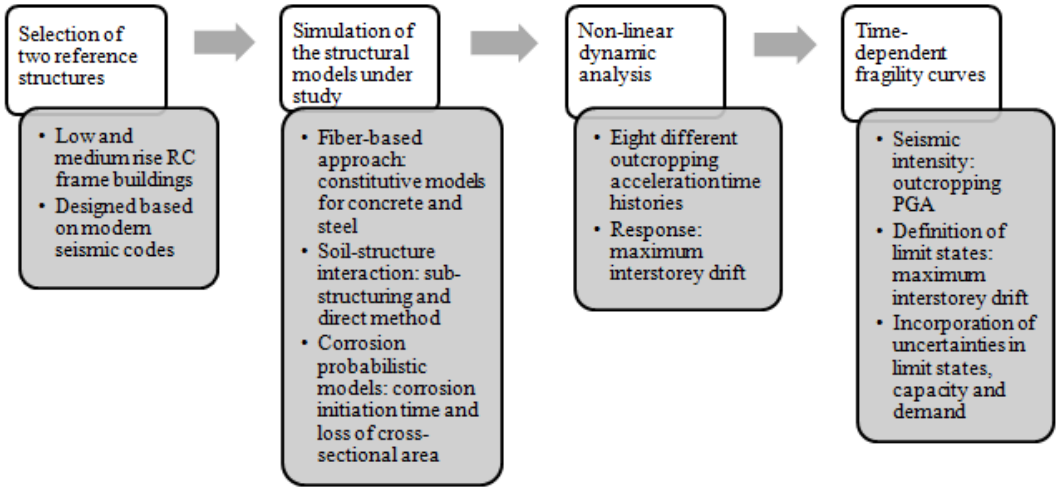

Figure1. Methodological framework adopted in this study.

2 METHODOLOGY

2.1 Description of structural models

Two reference moment resisting frames (MRFs), designed on the basis of modern seismic codes are selected for the present study. The first one [8] is a two storey – one bay frame model that is considered representative of low – rise buildings designed by the Greek seismic code [9]. The second one is a four storey frame model with three bays [10] that is considered to be representative of mid – rise buildings designed based on the modern seismic code of Portugal (Figure 2). Table 1 represents some of the main characteristics of the reference models such as the fundamental period and the strength of concrete and steel. The main analytical modeling of the structures is conducted using the Open System for Earthquake Engineering Simulation (OpenSees) software [11], an object-oriented open source software framework for finite element analysis developed by PEER. In addition, the finite element code Seismostruct [12] is used to enhance the reliability of the analysis and to permit correlations on the seismic structural response and fragility.

The OpenSees platform is designed around an object-oriented architecture facilitating the use of existing features and the development of new components, making it particularly attractive for the modeling of complex structural or geotechnical systems subjected to static or dynamic loading. An extensive library of material models and non-linear elements are provided, supporting also a wide range of solution procedures and computation models. Inelastic force-based formulations are employed for the simulation of the nonlinear beam-column frame elements considering four Gauss-Lobatto[13] integration points along each member's length. The applied formulations allow both geometric and material nonlinearities to be captured. Distributed material plasticity along the element length is considered based on the fiber approach to represent the cross-sectional behavior [14]. Each fiber is associated with a uniaxial stress-strain relationship and the sectional stress-strain state of the beam-column elements is obtained through the integration of the nonlinear uniaxial stress-strain response of the individual fibers in which the section is subdivided. The fiber section has a general geometric configuration formed by sub-regions including the concrete patches of simple regular quadrilateral shapes and the reinforcement layers. Concrete and steel fiber behaviors may be modeled and defined in the direction of each member length representing the flexural component in the fiber based analysis. Modified Kent and Park model [15] is used to define

the behavior of the concrete fibers, yet different material parameters are adopted for the confined (core) and the unconfined (cover) concrete.

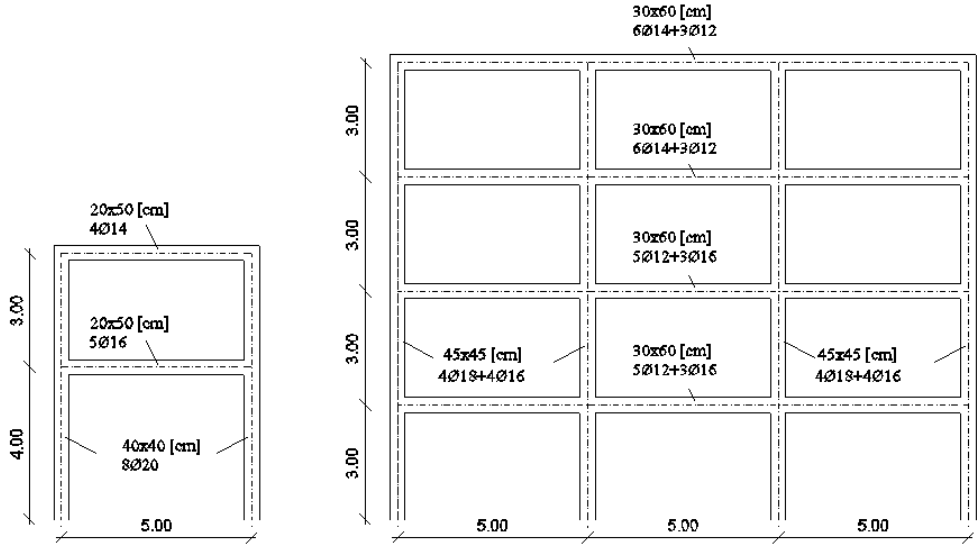

Figure 2. Reference MRF models used for time – dependent vulnerability assessment

RC building		Sections [cm]	Mass [t/m]	Fundamental period T[sec]	f_c [MPa]	f_y [MPa]
Low-rise	Column	40x40	0.41	0.3936	20	500
	Beam 1st - 2nd floor	20x50	3.15			
Mid-rise	Column	45x45	0.51	0.5018	28	460
	Beam 1st - 2nd - 3rd floor	30x60	4.77			
	Beam 4rth floor	30x60	3.41			

Table 1. Characteristics of the studied buildings

The uniaxial 'Concrete01' material is used to construct a uniaxial Kent-Scott-Park concrete material object with degraded linear unloading/reloading stiffness according to the work of Karsan-Jirsa [16] with zero tensile strength. The steel reinforcement is modeled using the uniaxial 'Steel01' material to represent a uniaxial bilinear steel material object with kinematic hardening with no isotropic hardening described by a nonlinear evolution equation (Figure 3).

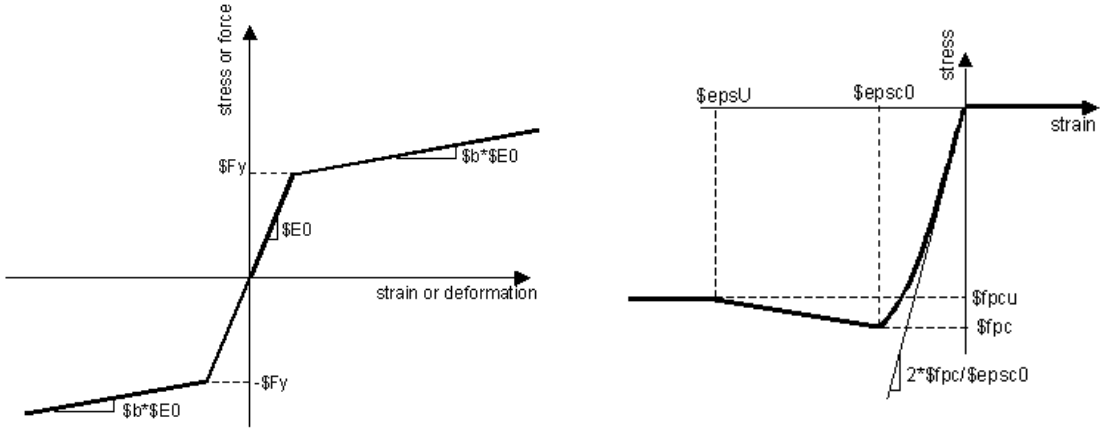

Figure 3. 'Steel 01' (left) and 'Concrete01' (right) material properties (Mazzoni et al. 2009)

2.2 Soil-structure interaction modeling

For the reference structural models fixed base conditions are considered assuming that they are founded on rigid rock (see fig. 4 (a)). For the SSI models, two different approaches are applied, namely the direct (see fig. 4 (b)) and the substructure method (see figs. 4 (c) and (d)). The applied modelling approaches are summarized in Figure 4. A representative soil profile with an average low strain velocity $V_{so,ave}$ taken equal to 300m/sec is used for the SSI simulations as illustrated in Figure 5.

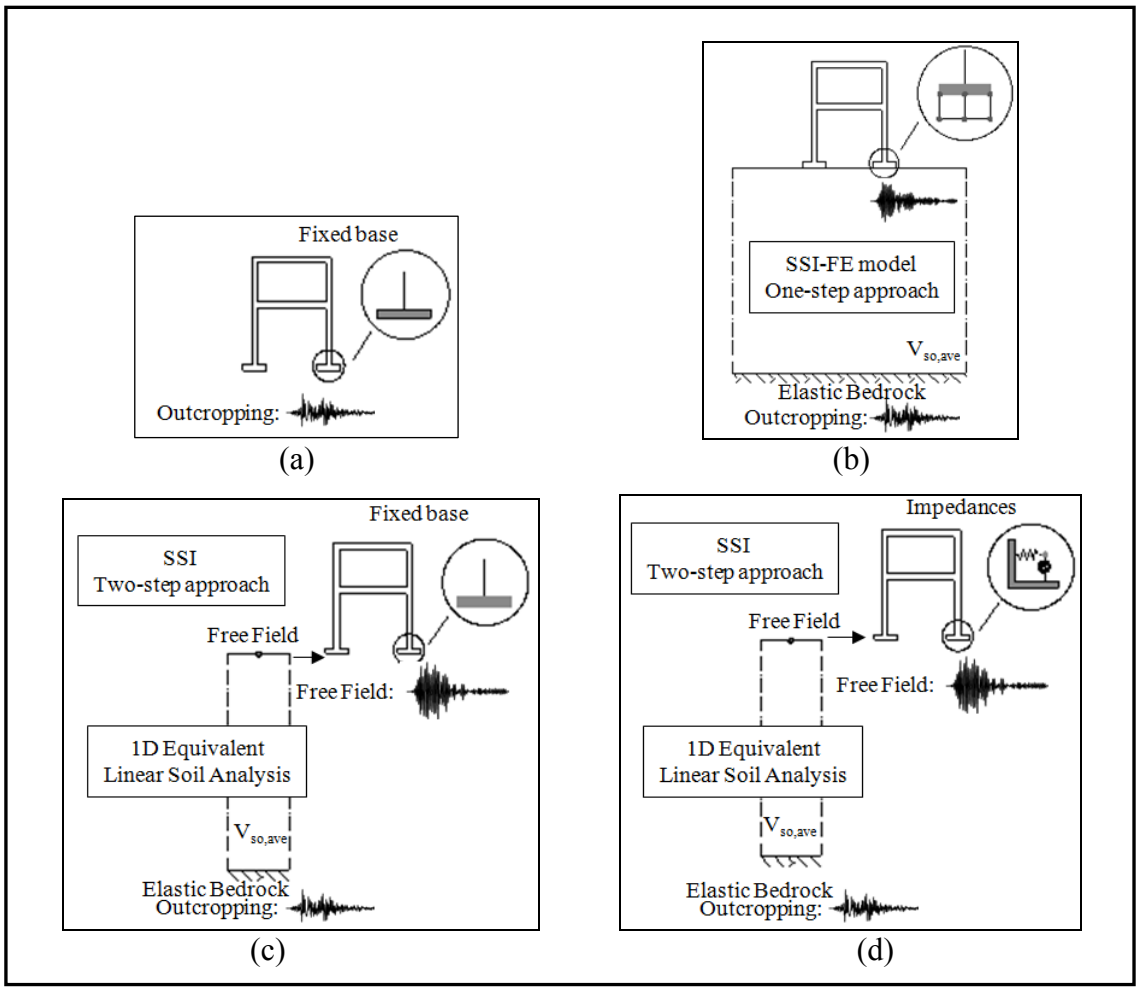

Figure 5. Schematic view of the applied approaches

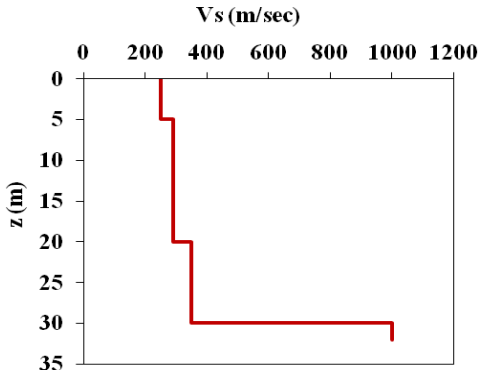

Figure 4. Properties of considered soil profile

2.2.1 Two-step analysis

In the two-step approach the coupling of the two sub models (soil and structure) is achieved by introducing appropriate impedance functions (e.g. rotational/translational springs and dashpots) into the base of the structural models. For the outcropping seismic motion, one – dimensional equivalent linear analyses for the given soil profile (corresponding to shear wave velocity V_{so}=300m/sec) (see fig. 4) are performed using Cyberquake [17] to obtain the free field motion which is subsequently imposed as input motion at the base of the structures. The consideration of an elastic half space (elastic bedrock Vs=1000m/sec), which is assumed 30m beneath the ground surface, allows applying directly the outcropping rock motion at the base of the soil model [18]. The shear modulus reduction and damping curves proposed by Darandeli [19] are used to model the strain depended soil nonlinearity. Following the equivalent linear soil formulation, the effective shear strain amplitude of the surface layer ($\gamma_{eff}=0.65\cdot\gamma_{max}$) is used for the calculation of the new compatible shear modulus and material damping ratio values. Subsequently, based on the new dynamic soil properties, coupling impedances proposed by Mylonakis et al. [20] for surface foundation on homogeneous halfspace are estimated. The dimensions of the footings are 1.7m x 1.7m and 2.0m x 2.0m for the low and medium rise structures respectively according to modern seismic code standards. The non-linear dynamic analyses of the considered structures are then conducted using the FE code Seismostruct [12] (see [3] for details).

2.2.2 One-step analysis

A general schematic view of the considered soil-structure model used for the one step approach is illustrated in Figure 6. OpenSees is used for the finite element modeling of the soil-structure system. The soil is modeled in two-dimensions with two degrees-of-freedom using the plane strain formulation of the quad element. To account for the finite rigidity of the underlying half-space, a Lysmer-Kuhlemeyer [21] dashpot is incorporated at the base of the soil profile. The soil profile is excited at the base by a horizontal force time history which is proportional to the known velocity time history of the ground motion ([22], [23]). The soil profile model adopted in this study has a total length of 120m and width of 30m and includes approximately 3600 four-node quadrilateral elements. The geometry of the mesh is based upon the concept of resolving the propagation of the shear waves at or below a particular frequency by ensuring that an adequate number of elements fit within the wavelength of the chosen shear wave. This ensures that the mesh is refined enough such that the desired aspects of the propagating waves are well captured in the analysis. Considering that the maximum frequency of interest is 10Hz and adopting a relatively dense discretization, quad elements with dimensions 1.0m x 1.0m are implemented. Even though soil material nonlinearity can be incorporated in the direct approach, in this study elastic soil layers are considered that are calibrated in terms of modulus of elasticity and Rayleigh damping, based on the response of the 1D equivalent linear soil analyses conducted in CyberQuake for the sub-structure method, to allow for direct comparison of the two SSI modeling approaches. The elastic bedrock (Vs=1000 m/sec) lies at 30 m beneath the ground surface. The Lysmer-Kuhlemeyer [21] dashpot is defined based on the viscous uniaxial material model and the zeroLength element formulation used to connect the two previously defined dashpot nodes. The connection of the soil and the structure is achieved by applying common nodes and appropriate constrains (to ensure equal displacement) for both the soil and structure's footings that are modeled as rigid beam-column elements.

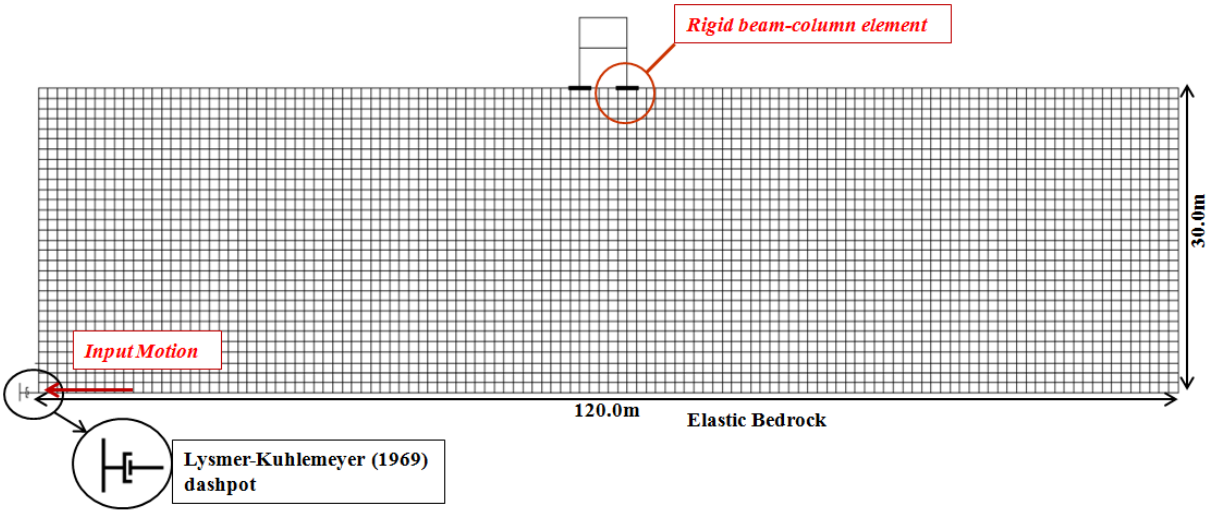

Figure 6. OpenSees 2D soil-structure model

2.3 Corrosion modeling

Several models have been proposed to quantify structural degradation due to corrosion that may be applied within the vulnerability analysis framework. A summary of these models can be found in DuraCrete [24]. In this study corrosion of reinforcing steel due to the ingress of chloride ions from the concrete surface to the steel bars is investigated. The probabilistic model proposed by FIB- CEB Task Group 5.6 [25] is adopted herein to determine the corrosion initiation time due to chloride ingress:

$$T_{ini} = \left(\frac{\alpha^2}{4 \cdot k_e \cdot k_t \cdot D_{RCM,0} \cdot (t_0)^n} \cdot \left(erf^{-1}\left(1 - \frac{C_{crit}}{C_s}\right)\right)^{-2} \right)^{\left(\frac{1}{1-n}\right)} \quad (1)$$

where T_{ini}=corrosion initiation time (years), α =cover Depth (mm) $C_{crit.}$=critical chloride content (wt % cement); C_s = the equilibrium chloride concentration at the concrete surface (wt % cement); t_0= reference point of time (years); $D_{RCM,0}$=Chloride migration Coefficient (m^2/s); k_e=environmental function; k_t=regression parameter; *erf*=Gaussian error function and n=aging exponent.

Once the protective passive film around the reinforcement dissolves due to continued chloride ingress, corrosion initiates and the time dependent loss of reinforcement cross-sectional area can be expressed as (e.g. [5]):

$$A(t) = \begin{cases} n \cdot D_i^2 \cdot \dfrac{\pi}{4} & \text{for } t \le T_{ini} \\ \max\left[n \cdot \left(D \cdot (t)\right)^2 \cdot \dfrac{\pi}{4},\ 0 \right] & \text{for } t \ge T_{ini} \end{cases} \quad (2)$$

where n=number of reinforcement bars; D_i=initial diameter of steel reinforcement; t=elapsed time in years and D(t)=reinforcement diameter at the end of ($t - T_{ini}$) years, which can be defined as:

$$D(t) = D_i - i_{corr} \cdot \kappa \cdot (t - T_{ini}) \quad (3)$$

where i_{corr}=rate of corrosion (mA/cm^2); κ =corrosion penetration (μm/year) (κ =11, 6μm/year uniform corrosion penetration for generalized corrosion).
The statistical quantification of the model parameters involved within the calculation of the chloride induced corrosion initiation time adopted for the present study is given in Table 2 based on FIB- CEB Task Group 5.6 (2006) prescriptions and the available literature (e.g. [26], [27], [5]). The chloride exposure condition considered is a relatively aggressive atmospheric exposure environment (e.g. k_e=0.67, [6]) corresponding to an adverse chloride induced deterioration scenario (w/c=0.6, high corrosion level). A lognormal distribution for the corrosion initiation time with a mean value of 2.96 years and standard deviation of 2.16 years is estimated based on crude Monte Carlo simulation that is found to be a good fit to the simulated data for the corrosion initiation time (Figure 7).

Parameter	Mean	COV	Distribution
Cover Depth (mm) α	25	0.20	Lognormal
Environmental transfer variable k_e	0.67	0.10	Normal
Chloride migration Coefficient ($D_{RCM,0}$) (m^2/s)	2.5E-11	0.10	Normal
Aging exponent n	0.3	cov=0.05, a=0.0, b=1.0	Beta
Critical Chloride Concentration (C_{cr}) wt % cement	0.6	cov=0.05, a=0.2, b=2.0	Beta
Surface Chloride Concentration (C_s) wt % cement	1.539	0.10	Normal
Rate of Corrosion (i_{corr}) mA/cm^2	10	0.20	Normal

Table 2. Statistical characteristics of the parameters affecting the chloride induced corrosion deterioration of RC elements adopted in the present study

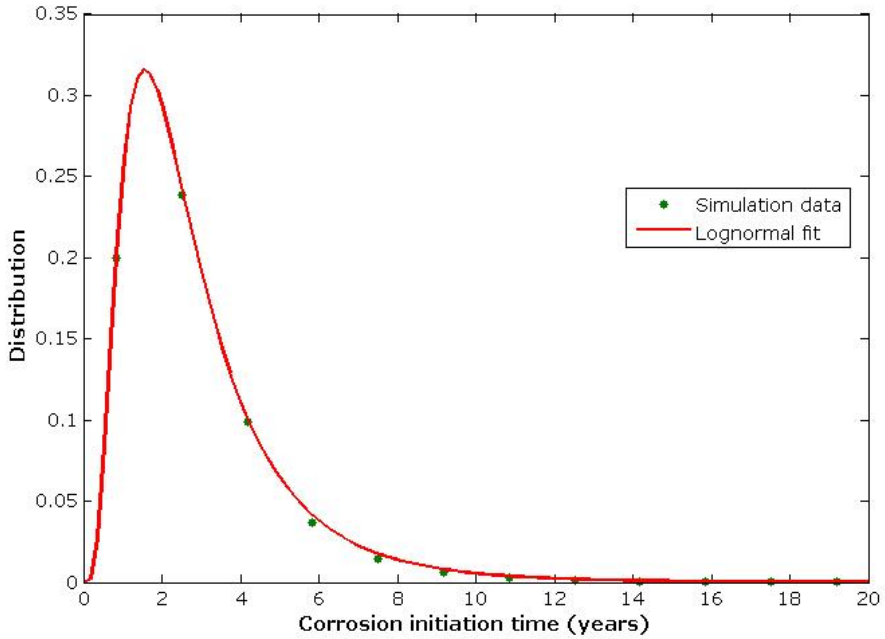

Figure 7. Lognormal distribution of chloride corrosion initiation time T_{ini} (mean = 2.96 years, Standard Deviation = 2.16 years.

Table 3 presents the loss of reinforcement area due to corrosion within the elapsed time ($t-T_{ini}$). It is assumed that the loss of steel area is uniformly distributed along the reinforced concrete members whereas neither the degradation of steel material properties nor the cover concrete strength reduction are taken into account.

RC Building	Element	Reinforcement (t=0 years)	Reinforcement area		Loss of Reinforcement area at t=50 years
			Ao (t=0years) (mm^2)	A(t=50years) (mm^2)	A(t)/Ao
Low-rise	Column	8Φ20	2513.20	1340.00	0.53
	1st floor beam	5Φ16	1005.31	447.65	0.45
	2nd floor beam	4Φ14	615.75	238.72	0.39
Mid-rise	Column	4Φ18	1017.88	502.78	0.49
		4Φ16	804.25	358.14	0.45
	1st and 2nd floor beams	2Φ10	157.08	37.99	0.24
		5Φ12	565.49	180.59	0.32
		3Φ16	603.19	268.62	0.45
	3rd and 4th floor beams	6Φ10	471.24	113.86	0.24
		3Φ12	339.29	108.22	0.32

Table 3. Reinforcement area in different points in time (t= 0 and 50 years) for the low and mid-rise RC buildings

3 NONLINEAR TIME-HISTORY ANALYSES

In order to study the SSI and aging effects on the behavior of the reinforced concrete frames under dynamic loading, 2-dimensional nonlinear time-history analyses are performed to determine the inelastic seismic response of the un-corroded (t=0 years) and corroded (t=50 years) structures to a series of earthquake records of varying intensity. Eight different ground motion records are selected as input excitation for the analyses performed in the present study. They are all referring to outcrop conditions recorded at sites classified as rock or stiff soil according to EC8 (Table 4). In Figure 8 the normalized elastic response spectra of the records is illustrated in comparison to the proposed elastic design spectrum of EC8 [28] for soil type A (rock). Each ground motion is progressively scaled to three different levels of peak ground acceleration PGA (0.1, 0.3 and 0.5g) to capture the variability in seismic demand prediction and the effect of different characteristics of earthquake ground motion (amplitude, frequency content, duration) on the structural dynamic response in relation to the dynamic properties of soil and structure.

Various parameters are investigated such as the top-floor acceleration and displacement histories, the peak ground acceleration PGA and the spectral acceleration $S_a(T)$ (at fundamental period of the structure) at the base and top of the models and the transfer functions with respect to the frequency content of the input motion. The output response parameter used in this study as a damage index in the seismic fragility analysis is the maximum inter-storey drift ratio (ISD_{max}%).

Earthquake	Record station	Mw	R (km)	PGA (g)
Valnerina, Italy 1979	Cascia	5.9	5.0	0.15
Friuli, Italy 1976	San Rocco	5.9	15.0	0.11
Parnitha, Athens 1999	Kypseli	6.0	10.0	0.12
Montenegro 1979	Hercegnovi Novi	6.9	60.0	0.26
Northridge, California 1994	Pacoima Dam	6.7	19.3	0.42
Palm Springs, California 1986	Whitewater Trout Farm	6.2	7.3	0.52
Campano Lucano, Italy 1980	Sturno	7.2	32.0	0.32
Umbria, Italy 1998	Cubbio-Piene	4.8	10.0	0.24

Table 4. List of outcropping records used for the dynamic analysis

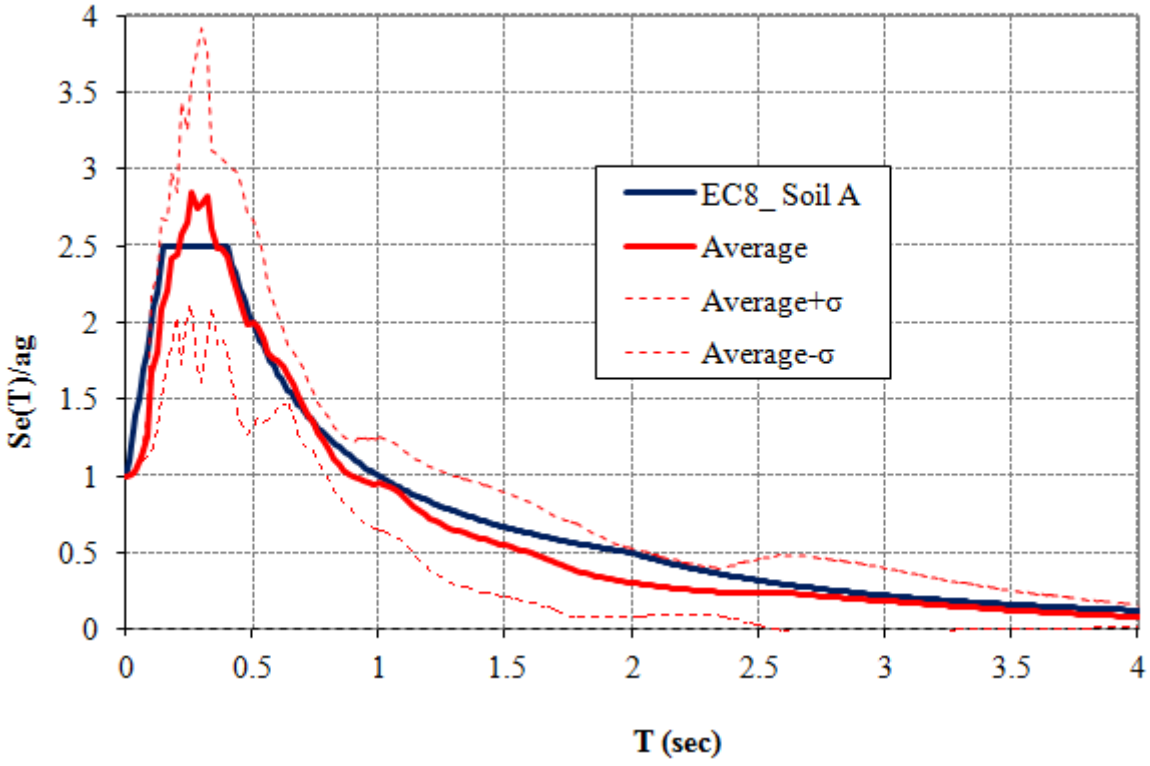

Figure 8. Normalized average elastic response spectrum of the input motions in comparison with the corresponding elastic design spectrum for soil type A (rock) according to EC8

4 TIME-DEPENDENT FRAGILITY CURVES

Fragility curves represent graphical relationships yielding the probability of exceeding a certain level of damage under an excitation of certain intensity. The selection of well-defined and realistic damage states is a key parameter in the development of seismic fragility curves. The selection in the present study of the maximum inter-storey drift ratio (ISD_{max}%) as a global measure of damage is made because it is a comprehensive and easily calibrated indicator and as that it has been widely used in similar studies. Four damage states (slight, moderate, extensive, complete) are defined based on the drift limits proposed by Ghobarah [39]. Under the reasonable assumption that the corroded structures (t=50 years) present limited ductility compared to their initial non-corroded state (t=0 years), different drift limits are adopted for each time scenario. On this basis, the limit values corresponding to ductile

moment resisting frames (MRFs) are assigned to the non-corroded structures whereas for the corroded ones the drifts corresponding to the non-ductile MRFs are adopted (Table 5).

State of damage	Ductile MRF	Nonductile MRF
Slight/Light damage	0.4	0.2
Moderate damage	1.0	0.5
Extensive damage	1.8	0.8
Complete	3.0	1.0

Table 5. Damage states for Ductile and nonductile MRFs used in this study (after [30])

The time dependent fragility functions of the buildings can be mathematically expressed as two-parameter time-variant lognormal distributions:

$$P\left[DS / IM\right] = \Phi\left(\frac{In\left(IM\right) - In\left(\overline{IM}\left(t\right)\right)}{\beta\left(t\right)}\right) \tag{3}$$

where, Φ is the standard normal cumulative distribution function, IM is the intensity measure of the earthquake expressed in terms of PGA (in units of *g)* at the ground surface, $\overline{IM}\left(t\right)$ and β(t) are the median values (in units of *g)* and logarithmic standard deviations of the building fragilities at different points in time along its service life and *DS* is the damage state. The median values of PGA corresponding to the prescribed damage limit states are determined based on a regression analysis of the nonlinear dynamic analyses results (PGA (g) and ISD_{max}(%)) for each structural model and time scenario (t=0 and 50 years). In Figure 9 representative PGA - ISD_{max}% relationships are illustrated for the low rise structure considering fixed and flexible (SSI effect for $V_{so,ave}$ =300m/s) foundation conditions for the initial (t=0 years) and corroded (t=50 years) scenario.

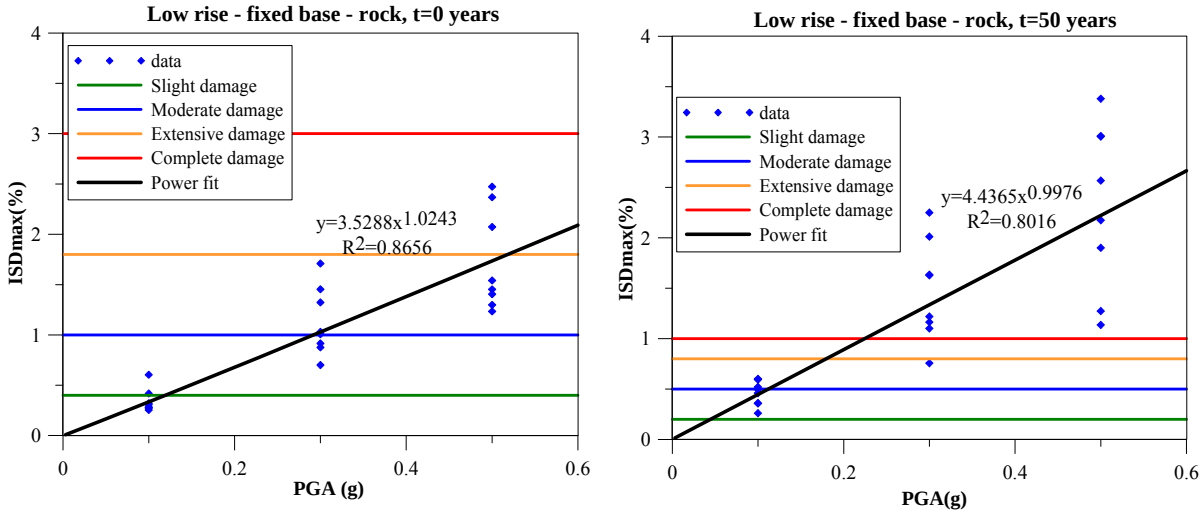

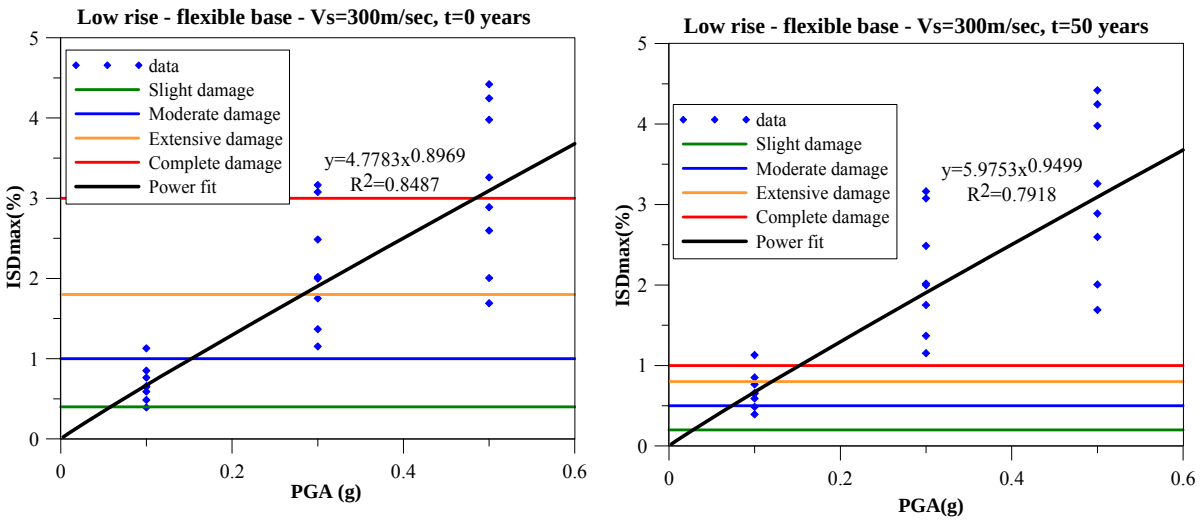

Figure 9. PGA-ISD_{max}(%) relationships for the low rise structures considering fixed and compliant condition for the initial and corroded scenario.

The various uncertainties are taken into account through the log-standard deviation parameter β(t), which describes the total dispersion related to each fragility curve. Three primary sources of uncertainty contribute to the total variability for any given damage state (NIBS, 2004), namely the variability associated with the definition of the limit state value, the capacity of each structural type and the seismic demand. The uncertainty in the definition of limit states is assumed to be equal to 0.4 while the variability of the capacity is assumed to be 0.25 (NIBS, 2004). The third source of uncertainty associated with the demand, is taken into consideration by calculating the variability in the results of the numerical simulations. Under the assumption that these three variability components are statistically independent, the total variability is expressed as the root of the sum of the squares of the component dispersions.

5 RESULTS AND DISCUSSION

In Figures 10 and 11, the derived fragility curves for the fixed and the flexible base (compliant foundation) structures are compared. For the fragility curve set referring to the flexible base models, in both aforementioned figures, soil structure interaction is taken into account based on the one-step direct method (modeling approach b in Figure 4). Regarding the reference fixed base structures, foundation on rigid rock is assumed in Figure 10 by directly imposing the outcropping input motion whereas a modified input excitation due to the considered soil profile is taken into account in Figure 11 (modeling approach a and c in Figure 4 respectively). It is seen that the consideration of soil-foundation compliance and SSI effects may significantly increase the structure's fragility in relation to the fixed-base case. Moreover the increase in vulnerability appears to be higher for the sub-structure in comparison to the direct method of SSI simulation (Figure 12). On the contrary, studying soil-structure interaction effects may result to a slight decrease in vulnerability compared to the fixed-base models, when for the later ones the modified input motion due to the underlying soil profile is considered. This decrease seems to be more pronounced in the case of the one-step approach of SSI modeling (Figure 13). These remarks may be attributed to the fact that in the two-step approach the effect of radiation damping as a result of soil nonlinearity is generally neglected in contrast to the direct one-step method where both hysteretic and radiation damping are taking place simultaneously. Modeling uncertainties associated with the

two different codes used for the uncoupled and coupled SSI analysis (Seismostruct and Opensees respectively) may have also contributed to the observed differences in seismic fragility. Similar trends are expected to occur for both low and mid-rise structural configurations. Overall, it should be noted that the consideration of SSI and site effects may either increase or decrease the expected structural damage depending on the type of the structure, ints foundation system and its fundamental period in relation to the dynamic input motion and the soil dynamic properties.

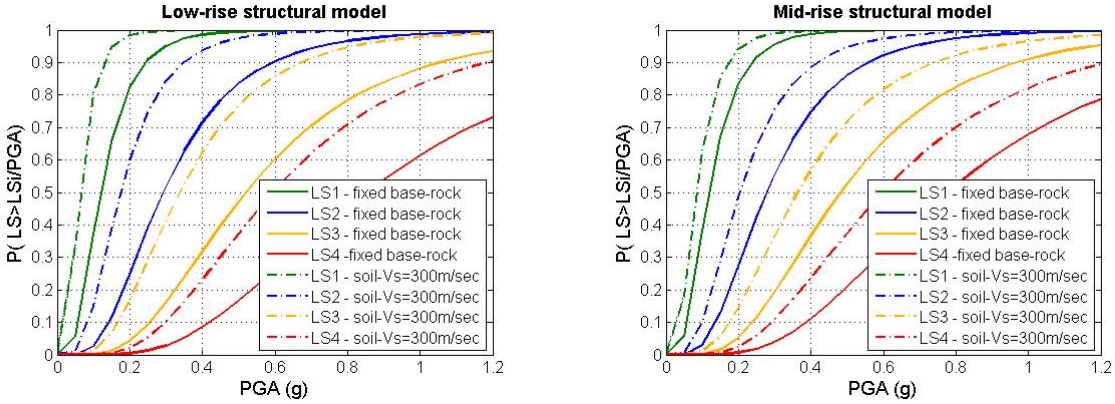

Figure 10. Comparison of fragility curves for the low rise (left) and mid-rise (right) structures considering fixed and compliant (Vs=300m/sec) foundation condition for the initial (t=0years) scenario.

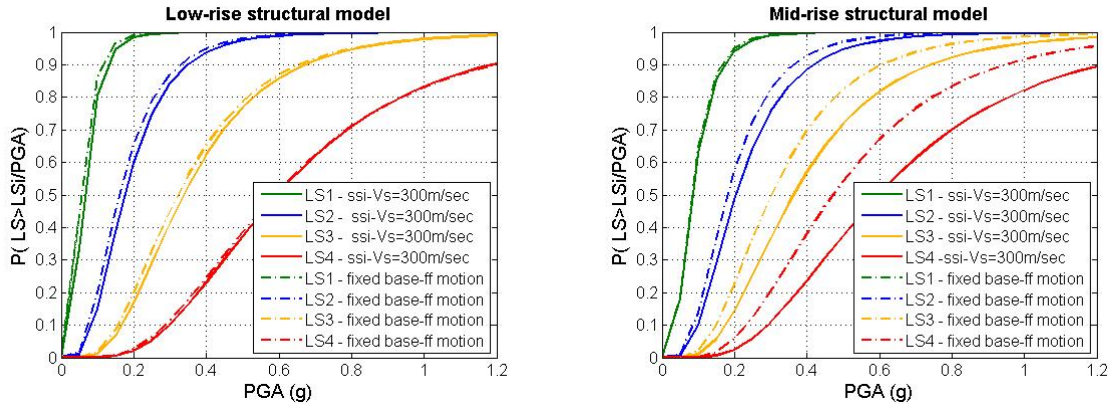

Figure 11. Comparison of fragility curves for the low rise (left) and mid-rise (right) structures considering fixed foundation with free field input motion and flexible foundation and soil structure interaction effects for the initial (t=0years) scenario.

Furthermore Figure 14 illustrates the derived sets of fragility curves for the different building configurations for the initial non-degraded state, compared to the corresponding curves when considering corroded structural members. As expected, for both low and mid-rise building typology, the fragility curves for the corroded structures display a great shift to lower acceleration values for the same earthquake scenario indicating a significant increase due to aging. The large differences observed between the curves for un-corroded and corroded frame buildings could be attributed to the most adverse deterioration scenario adopted herein to better illustrate the phenomenon. It is also attributed to the different damage state thresholds adopted for the initial and corroded structure, which again may be considered as an extreme case (see Table 5). Table 6 presents the corresponding median and beta values of each damage state for all the building configurations and time scenarios analyzed.

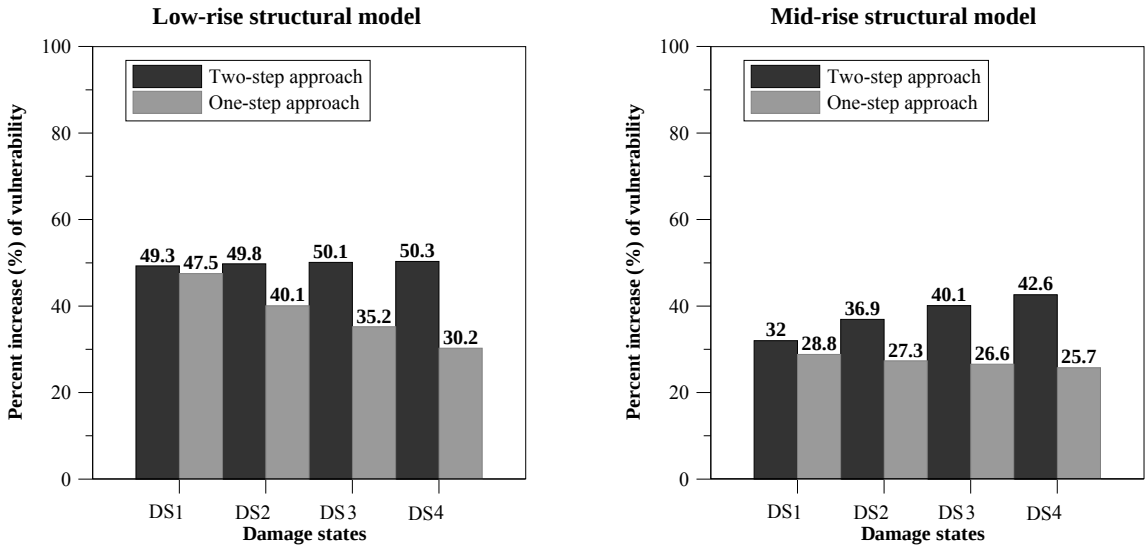

Figure 12. Comparison of the percent increase in vulnerability for the low rise (left) and mid-rise (right) with flexible foundation structures for the sub-structure (two-step) and the direct (one-step) method of SSI modeling in relation to the fixed base models.

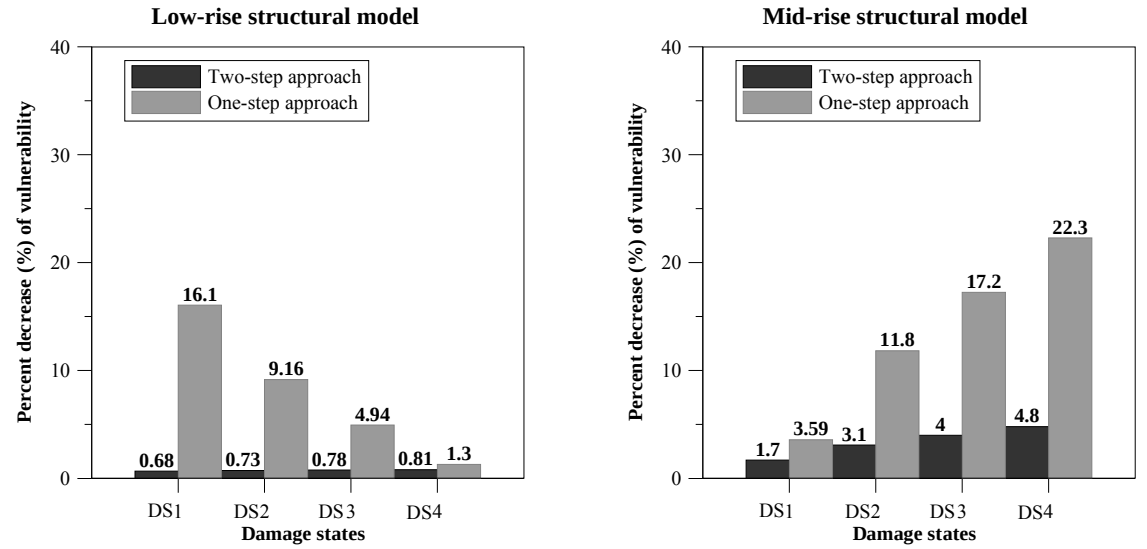

Figure 13. Comparison of the percent decrease in vulnerability for the low rise (left) and mid-rise (right) with flexible foundation structures for the sub-structure (two-step) and the direct (one-step) method of SSI modeling in relation to the fixed base models with free field input motion.

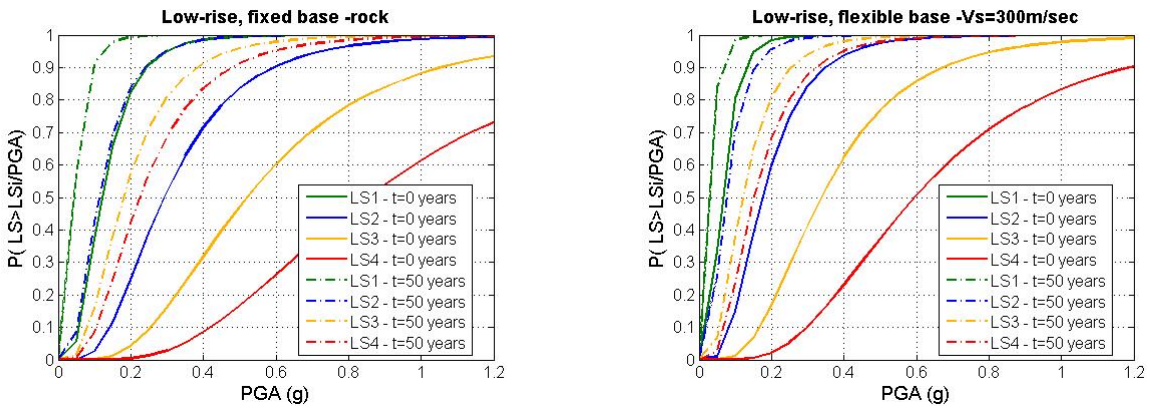

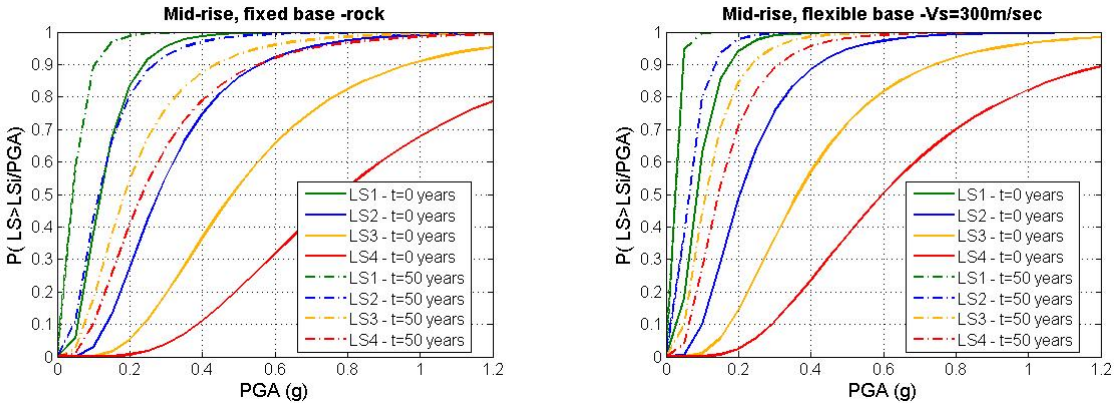

Figure 14. Fragility curves for the low rise (left) and mid-rise (right) structures considering fixed and compliant (Vs=300m/sec) foundation conditions for the initial (t=0 years) and the corroded (t=50 years) scenario)

RC building	Foundation conditions	Time scenario (years)	Median PGA (g)				Dispersion
			Slight	Moderate	Extensive	Complete	
Low-rise	Fixed base - rock	t=0	0.12	0.29	0.52	0.85	0.551
		t=50	0.05	0.11	0.18	0.23	0.588
	Flexible base V_{so}=300 m/s	t=0	0.06	0.18	0.34	0.6	0.538
		t=50	0.03	0.07	0.12	0.15	0.585
Mid-rise	Fixed base - rock	t=0	0.12	0.28	0.48	0.78	0.544
		t=50	0.04	0.11	0.19	0.23	0.668
	Flexible base V_{so}=300 m/s	t=0	0.08	0.2	0.36	0.6	0.557
		t=50	0.02	0.06	0.11	0.14	0.599

Table 6. Parameters of fragility functions

6 CONCLUSIONS

The seismic vulnerability of RC frame buildings has been assessed taking into account foundation compliance and SSI effects as well as the corrosion of the RC structural members. Two low and mid-rise bare frame structures were analyzed using 2D nonlinear dynamic computations. Time-dependent probabilistic fragility functions have been derived for predefined damage states for two time periods (t=0, 50 years) in terms of outcropping peak ground acceleration. The results indicate an overall increase in the structure's vulnerability when soil deformability and foundation compliance are taken into account. However, this should not be regarded as a general trend as the seismic structural vulnerability may decrease or increase depending on the characteristics of the buildings, the input motion and the soil properties. Furthermore when the modified input motion due to the underlying soil profile is used for the anlysis of the fixed base models, a slight decrease in structure's fragility is observed when soil-structure interaction is taken into account. The comparison of the two SSI modeling techniques indicates that the uncoupled two-step approach (substructure method) leads to higher vulnerability levels, certainly due to uncertainties related, among others, to the evaluation of the foundation impedances. A significant increase in the seismic fragility of the structures is observed over time due to the consideration of aging effects (corrosion). This important increase is due to the voluntary selection of the "worst cas scenario" for the damage

states and the corrosion process. In order to increase the robustness of the conclusions presented herein, further research is needed in the definition of limit states for corroded structures based on adequate analytical, experimental and empirical data and in the incorporation of the fully probabilistic corrosion models within the dynamic analysis. In summary, the results presented in this paper prove that the seismic fragility curves used so far for RC buildings considering fixed base conditions and assuming no aging effects, may, under certain circumstances, underestimate the real vulnerability of the structures.

AKCNOWLEDGEMENT

Most of the work reported in this paper was carried out in the framework of the ongoing REAKT (http://www.reaktproject.eu/) project, funded by the European Commission, FP7-282862.

REFERENCES

[1] National Institute of Building Sciences, *Direct physical damage – General building stock,* HAZUS-MH Technical manual, Chapter 5, Federal Emergency Management Agency, Washington, D.C.

[2] E. Saez, Effect of the inelastic dynamic soil-structure interaction on the seismic vulnerability assessment, *Structural Safety,* **33**, 51-63, 2011.

[3] S.D. Fotopoulou, S.T. Karapetrou, K.D. Pitilakis, Seismic vulnerability of RC buildings considering SSI and aging effects, *15WCEE International Conference*, Lisboa, 2012.

[4] DuraCrete, *Probabilistic performance based on durability design of concrete structures: Statistical quantification of the variables in the limit state functions,* Report No.: **BE 95-1347**, 62-63, 2000.

[5] J. Ghosh, J.E. Padgett, Aging considerations in the development of time-dependent seismic fragility curves, *Journal of Structural Engineering,* **136:12**, 1497-1511. 2010.

[6] D.E. Choe, P. Gardoni, D. Rosowsky, Fragility increment functions for deteriorating reinforced concrete bridge columns, *Journal of Engineering Mechanics,* **136:8**, 969-978, 2010.

[7] H. Yalciner, S. Sensoy, O. Eren, Time-dependent seismic performance assessment of a single-degree-of-freedom frame subject to corrosion, *Engineering Failure Analysis,* **19**, 109-122, 2012.

[8] F. Gelagoti, *Metaplastic Response and Collapse of frame-foundation systems, and the concept of rocking isolation*, Ph.D. Dissertation, National technical University of Athens, 2010.

[9] EAK2000, *Greek Seismic Code, Organization of Seismic Planning and Protection*, 2000.

[10] A. Abo El Ezz, *Deformation and strength based assessment of seismic failure mechanisms for existing RC frame buildings*, Master Dissertation, Rose School, Pavia, 2008.

[11] S. Mazzoni, F. McKenna, M.H. Scott, G.L. Fenves, *Open System for Earthquake Engineering Simulation User Command-Language Manual,* Pacific Earthquake Engineering Research Center, Berkeley, California, 2009.

[12] SeismoSoft, SeismoStruct, A computer program for static and dynamic nonlinear analysis of framed structures, (online): Available from URL: www.seismosoft.com , 2011.

[13] A. Neuenhofer and F.C. Filippou, Evaluation of nonlinear frame finite-element models, Journal of Structural Engineering, 123:7, 958-966, July, 1997

[14] E. Spacone, F.C. Filippou, F.F Taucer, Fibre beam-column element for nonlinear analysis of R/C frames, Part I: Formulation, *Earthquake Engineering and Structural Dynamics*, **25**, 711-725, 1996.

[15] D.C. Kent, R. Park, Flexural members with confined concrete, *Journal of the Structural Division*, Proc. Of the American Society of Civil Engineers, **97(ST7)**, 1969-1990, 1971.

[16] I. Karsan, J. Jirsa, Behavior of concrete under compressive loadings, *ASCE J. of the Structural Division*, **95**, 2543-2563, December, 1969.

[17] BRGM (French Geological Survey) Software Cyberquake, version 1.1, User's quide, 1998.

[18] A.O.L. Kwok, J.P. Stewart, Y.M. Hashash, N. Matasovic, R. Pyke, Z. Wang, Z. Yang, Use of exact solutions of wave propagation problems to guide implementation of nonlinear seismic ground response analysis procedures, Journal *of Geotechnical Engineering*, **133:11**, 1385-1398, 2007.

[19] M. Darendeli, *Development of a new family of normalized modulus reduction and material damping curves*, Ph.D. Dissertation, Univ. of Texas, 2001.

[20] G. Mylonakis, S. Nikolaou, G. Gazetas, Footings under seismic loading: Analysis and design issues with emphasis on bridge foundations, *Soil Dynamics and Earthquake Engineering,* **26**, 824-853, 2006.

[21] J. Lysmer, R.L. Kuhlemeyer, Finite dynamic model for infinite media, *J. Eng. Mech.*, **95**, 859-877, 1969.

[22] W.B. Joyner, A.T.F. Chen, Calculation of nonlinear ground response in earthquakes, *Bulletin of the Seismological Society of America*, 65:5, 1315-1336, October, 1975.

[23] J. Lysmer, *Analytical procedures in soil dynamics*, University of California at Berkeley, Earthquake Engineering Research Center, Richmond, **Report No. UCB/EERC-78/29**, CA, 1978.

[24] DuraCrete, Modeling of Degradation, BRITE-EURAM-Project BE95-1347/R4-5, 1998.

[25] CEB-FIB Task Group 5.6, Model for Service Life Design, fédération internationale du béton (fib), 2006.

[26] D.E. Choe, P. Gardoni, D. Rosowsky, T. Haukaas, Seismic fragility estimates for reinforced concrete bridges subject to corrosion, *Structural Safety* **31**, 275-283, 2009.

[27] M. Stewart, Spatial variability of pitting corrosion and its influence on structural fragility and reliability of RC beams in flexure, *Structural Safety*, **26**, 453-470, 2004.

[28] CEN-European Committee for Standarization prENV 1998-1 – Eurocode 8: design of structures for earthquake resistance. Part 1: deneral rules, seismic actions and rules for buildings, Draft No.4, Brussels, Belgium, 2003.

[29] A. Ghobarah, On drift limits associated with different damage levels, *International Workshop on Performance-Based Seismic Design*, Department of Civil Engineering, McMaster University, Ontario, Canada, June 28-July1, 2004.